NeoCAD Report—Prof. David J. Allstot

Executive Summary

As part of this project, parasitic-aware design and synthesis techniques for RF integrated circuits were developed using CAD schemes such as simulated annealing with tunneling, particle swarm optimization, and non-dominated sorting genetic algorithms. Computationally efficient methods for post-optimization process, voltage, and temperature (PVT) Monte-Carlo sensitivity analysis were also implemented. The parasitic-aware synthesis methodology was validated with its application to various RF circuit blocks including low-noise amplifiers, voltage-controlled oscillators and power amplifiers in CMOS and SiGe BiCMOS technologies.

For industry standard designs, this technique requires reliable circuit models for various active and passive components. Consequently, an approach for the fast and accurate generation of compact distributed circuit models for on-chip transmission lines on lossy silicon substrates was developed. This scheme uses a novel ABCD matrix partitioning procedure to extract these models from scattering parameters. The scattering parameters are obtained from measurements (and also supplemented by calibrated full-wave electromagnetic simulations) on a small set of transmission-line geometries spanning ranges of design parameter values. A feed-forward artificial neural network is trained using the extracted results, and applied to generate accurate models for arbitrary values within the bounds of the training ranges. As a result, the model generation time is greatly reduced compared to conventional approaches. The compact model generator is fully compatible with *HSPICE* and *SPECTRE-RF* and is easily incorporated into parasitic-aware RF circuit design and optimization tools.

Publications

1) D.J. Allstot, K. Choi, M. Mar, M. Rubeiz, C.-J. R. Shi, and R. Ward, "Parasitic-aware synthesis of CMOS RF power amplifiers via simultaneous topology selection and device sizing," *Intl. Conference on Communications Circuits and Systems*, 2002, pp. 1243-1247.

2) T. Kim, X. Li, and D.J. Allstot, "Compact model generation for on-chip transmission lines," *IEEE Trans. on Circuits and Systems I: Regular Papers*, vol. 51, pp. 459-470, March 2004.

3) D.J. Allstot, K. Choi, and J. Park, "Parasitic-aware Optimization of CMOS RF Circuits," Kluwer Academic Publishers, Boston, 2003. ISBN: 1402073992.

4) Taeik Kim, "A CMOS Tunable Transmission Line Phase Shifter and Voltage-Controlled Oscillator for Wireless Communications," *Ph.D. Dissertation,* University of Washington, March 1, 2004.

5) Hossein Zarei, "Smart Antenna Phase Shift Network Architectures and Circuits," *Ph.D. Dissertation,* University of Washington, Aug. 2004.

Students Trained

Taeik Kim
Hossein Zarei

Compact Model Generation for On-Chip Transmission Lines

Taeik Kim, *Student Member, IEEE*, Xiaoyong Li, *Student Member, IEEE*, and David J. Allstot, *Fellow, IEEE*

***Abstract*—An approach for the fast and accurate generation of compact distributed circuit models for on-chip transmission lines on lossy silicon substrates is presented. Using a novel ABCD matrix partitioning procedure, accurate distributed circuit models are extracted from scattering parameters obtained from measurements and calibrated full-wave electromagnetic simulations for a small set of transmission-line geometries spanning ranges of design parameter values. A feedforward artificial neural network is trained using the extracted results, and applied to generate accurate compact models for arbitrary values within the bounds of the training ranges. Consequently, the model generation time is greatly reduced compared to conventional approaches by exploiting the interpolation capabilities of the neural network. The compact model generator is fully compatible with *HSPICE* and *SPECTRE-RF* and is easily incorporated into parasitic-aware RF circuit design and optimization tools.**

***Index Terms*—ABCD matrix, coplanar waveguide, microstrip line, neural network, transmission line, transmission-line model.**

I. Introduction

OWING TO THE exponential rate of reduction of the minimum feature size of MOS transistors that has persisted for half a century, CMOS has emerged as a viable technology for system-on-chip (SOC) solutions integrating complex digital, precision analog, and multigigahertz radio frequency functions. Specific advantages of CMOS include low-power active devices with high transition frequencies (f_T), and low-cost high-volume manufacturing capabilities for mixed-signal/RF systems [1], [2]. Ironically, a major drawback of standard CMOS technology is that on-chip passive components limit RF circuit performance [3]. That is, conductive substrates and resistive metal interconnect layers impede the realization of high-Q inductors, transformers, etc.

Compact models of on-chip transmission lines (e.g., microstrip lines and coplanar waveguides) are needed for RF circuits operating above a few gigahertz [3], and fast and accurate compact model generators are desired in emerging parasitic-aware RF circuit design and optimization tools. Although transmission-line modeling is notoriously difficult owing to its complex multidimensional nature, several modeling methods have been presented. For example, transmission lines realized in a Si-SiO_2 system and represented by quasi-TEM, slow-wave, and skin-effect modes are experimentally characterized in [4]. Another widely used method of transmission-line characterization, full-wave electromagnetic simulation, achieves high accuracy at the expense of long computation times and large memory requirements [5]. Analytical equations based on conformal mapping techniques have been derived for simple transmission-line structures, but the requisite assumptions lead to inaccurate results; e.g., the assumption of an infinite substrate or a single dielectric layer is too simple for modern silicon technologies [6], [7]. In cases where a multilayer substrate is analyzed, simple approximate expressions for capacitance are used because accurate closed-form alternatives are intractable [8], [9]. Finally, a quasi-TEM spectral-domain approach that includes the effects of longitudinal substrate currents on inductance is described in [10]. While some of these approaches are compatible with commercial circuit simulators, they are generally neither fast enough nor accurate enough for use as compact model generators in parasitic-aware RF circuit synthesis tools that may require hundreds of thousands of iterations around an optimization loop to find an acceptable solution. For this critical application, fast and accurate compact model generators are needed that are directly compatible with circuit simulators such as *HSPICE, SPECTRE-RF*, etc.

In this paper, we present a comprehensive compact circuit model generation methodology for monolithic transmission lines. The approach is measurement based rather than physics based. Hence, it trades off physical understanding for accuracy by taking into account three-dimensional edge effects, layout asymmetries, process variations, etc. It comprises several steps. First, measured S-parameters are extracted from a small set of transmission lines spanning broad ranges of design parameter values (Fig. 1). The measured S-parameters are then used to "calibrate" an electromagnetic (EM) simulator; that is, one (or more) of its technology definition parameters (e.g., substrate resistivity) is empirically adjusted to achieve matching of the measured and EM-simulated results. The calibrated EM simulator is then used to generate accurate S-parameters for several more transmission lines coarsely interpolating the parameter ranges set by the measured results (Fig. 1). Note that although accurate, the calibrated EM simulator is much too slow for subsequent use in a parasitic-aware optimization loop. Next, accurate compact distributed circuit models are extracted for the set of measured and EM-simulated transmission lines and used to train a feedforward artificial neural network (ANN). Specifically, an ABCD matrix partitioning procedure is used

Manuscript received January 6, 2003; revised October 6, 2003. This work was supported in part by the U.S. Defense Advanced Research Project Agencies NeoCAD Program under Grant N66001-01-1-8919, in part by the National Science Foundation under Grant CCR-0086032 and Grant CCR-0120255, in part by the Semiconductor Research Corporation under Grant 2001-HJ-926 and Grant 2003-TJ-1093, in part by the National Semiconductor Corporation, and by Texas Instruments Incorporated. This paper was recommended by Associate Editor H. Graeb.

The authors are with the Department of Electrical Engineering, University of Washington, Seattle, WA 98195-2500 USA (e-mail: allstot@ee.washington.edu).

Digital Object Identifier 10.1109/TCSI.2003.822397

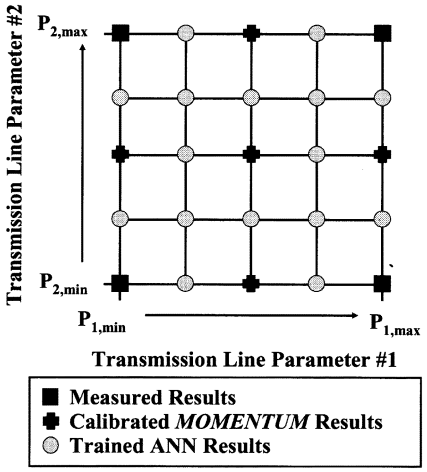

Fig. 1. Overall compact modeling methodology for an example transmission line with two design parameter ranges. Compact models are extracted from measured and calibrated EM-simulation results and used to train the neural network. The trained ANN quickly and accurately generates compact circuit models for arbitrary points within the parameter ranges.

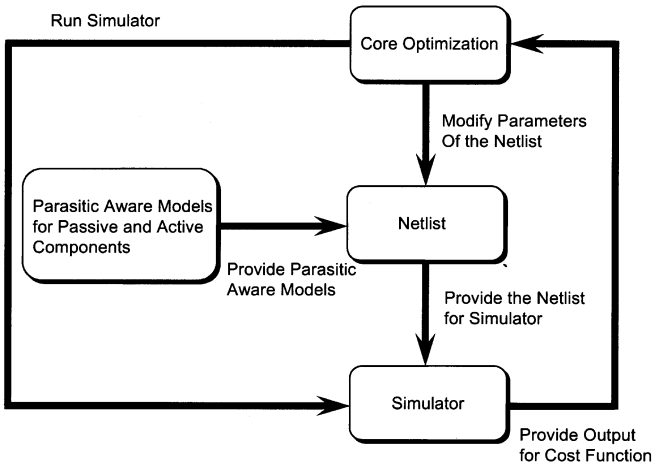

Fig. 2. Parasitic-aware design and optimization paradigm for RF integrated circuits. Key functional blocks include a core optimizer (simulated annealing, genetic, or particle swarm algorithms), a circuit simulator (*HSPICE* or *SPECTRE-RF*), and a fast and accurate passive circuit model generator.

to extract distributed circuit models from the S-parameters. After the neural network is trained, it generates compact models of transmission-line structures with arbitrary geometry sizes within the training ranges quickly and on the fly within a parasitic-aware design and optimization loop. Excellent agreement is exhibited between measured and calibrated *MOMENTUM* [11] results, and *HSPICE* simulations of the extracted distributed circuit models.

The paper is organized as follows. In Section II, the frequency-dependent characteristics of transmission lines are briefly reviewed. The ABCD matrix partitioning method for extracting an efficient compact model for a given transmission-line size, and comparisons between calibrated *MOMENTUM* simulations and distributed circuit model *HSPICE* results are presented in Section III. In Section IV, the artificial feedforward neural network technique used for fast and accurate compact model generation is described. Verification results from measurements are given in Section V with conclusions in Section VI.

II. Transmission-Line Characteristics

The parasitic-aware paradigm for RF circuit design and optimization with embedded passives such as transmission lines is depicted in Fig. 2. Parasitic-aware synthesis simply means that active and passive device and package parasitics are considered as part of an aggressive design and optimization process from the beginning. It has been demonstrated that the parasitic-aware methodology is essential for the synthesis of RF integrated circuits that must meet stringent specifications [12]–[14]. In practice, hundreds of thousands of iterations around the parasitic-aware optimization loop of Fig. 2 may be required to synthesize an RF circuit. Hence, it is imperative that the embedded compact circuit model generator is accurate and computationally efficient; conventional full-wave EM simulators are sufficiently accurate after calibration but too slow for use within the parasitic-aware optimization loop.

Cross sections of a coplanar waveguide and a microstrip line in CMOS and one *RLGC* section of a conventional compact distributed circuit model are shown in Fig. 3. The frequency-dependent *RLGC* distributed circuit model is valid over a wide range of frequencies under a quasi-TEM mode assumption [15]. A straightforward method of partitioning a transmission line into *RLGC* sections based on the Telegrapher equations is described in [16], [17]. In general, S-parameters, rather than small-signal Z- or Y-parameters, are typically used in EM simulators to maintain compatibility with commercial vector network analyzers that measure incident and reflected waves.

Using the Telegrapher equations, a cascade of a large number of identical *RLGC* sections with small series impedances $R(\omega)$ and $L(\omega)$, and shunt admittances $G(\omega)$ and $C(\omega)$, is required to accurately model a lossy transmission line. Specifically, the complex characteristic impedance Z, and the complex propagation constant γ, are related to the frequency-dependent *RLGC* section values per unit length of the transmission line as [16]

$$Z = \sqrt{\frac{[R(\omega) + j\omega L(\omega)]}{[G(\omega) + j\omega C(\omega)]}} \tag{1}$$

and

$$\gamma = \sqrt{[R(\omega) + j\omega L(\omega)][G(\omega) + j\omega C(\omega)]}. \tag{2}$$

The characteristic impedance and propagation constant are related to the S-parameters as [16]

$$Z = \sqrt{Z_0^2 \frac{(1 + S_{11})^2 - S_{21}^2}{(1 - S_{11})^2 - S_{21}^2}} \tag{3}$$

and

$$e^{-\gamma l} = \left\{ \frac{1 - S_{11}^2 + S_{21}^2}{2S_{21}} \pm K \right\}^{-1} \tag{4}$$

where

$$K = \sqrt{\frac{(S_{11}^2 - S_{21}^2 + 1)^2 - (2S_{11})^2}{(2S_{21})^2}}. \tag{5}$$

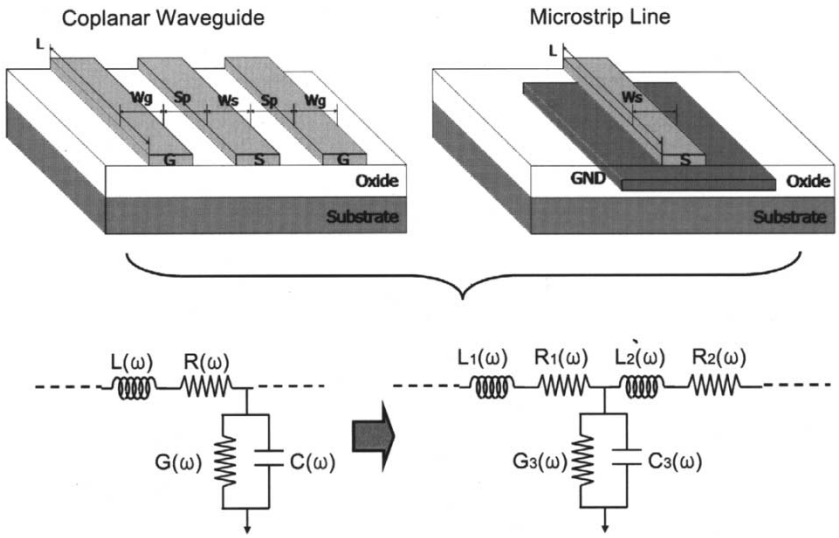

Fig. 3. Cross-sectional views of coplanar waveguide and microstrip line structures, and a distributed *RLGC* section and an equivalent T section derived using the Telegrapher equations. Many such sections are cascaded to form a distributed circuit model of the transmission line.

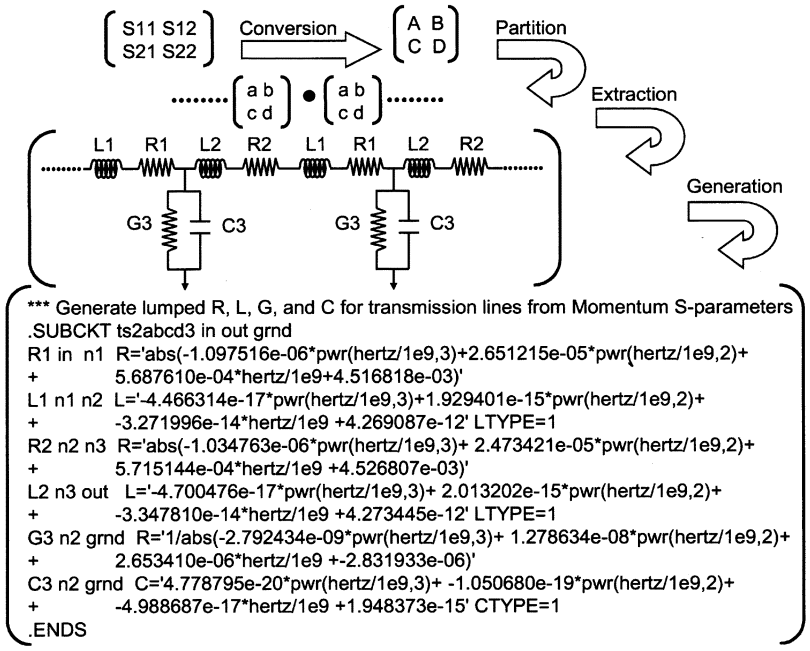

Fig. 4. Overview of the ABCD matrix partitioning method. The measured or EM-simulated S-parameter matrix is converted to an equivalent ABCD matrix, [ABCD]. N successive square roots of [ABCD] are taken to generate 2^N identical [abcd] matrices. Finally, [abcd] is converted into an equivalent T-cell using standard polynomial curve fitting techniques.

Knowing Z and γ, the series impedances $R(\omega)$ and $L(\omega)$, and shunt admittances $G(\omega)$ and $C(\omega)$ and per-unit length of transmission line are easily derived as [16]

$$R(\omega) = \mathrm{Re}(\gamma Z) \tag{6}$$

$$L(\omega) = \frac{\mathrm{Im}(\gamma Z)}{\omega} \tag{7}$$

and

$$G(\omega) = \mathrm{Re}\left(\frac{\gamma}{Z}\right) \tag{8}$$

$$C(\omega) = \frac{\mathrm{Im}\left(\frac{\gamma}{Z}\right)}{\omega}. \tag{9}$$

The method has several drawbacks. First, an *RLGC* section derived using the Telegrapher equations is inherently asymmetric as shown in Fig. 3; however, transformation to the equivalent T model with $R_1(\omega) = R_2(\omega) = 0.5R(\omega)$ and $L_1(\omega) = L_2(\omega) = 0.5L(\omega)$ achieves symmetry. While some transmission lines are ideally symmetric, the actual implementations are somewhat asymmetric owing to inherent layout asymmetries, process, voltage, and temperature variations, etc. The ABCD matrix method introduced herein produces an accurate distributed circuit model for symmetric and moderately asymmetric structures. Moreover, in the conventional approach, many distributed symmetric *RLGC* T sections must be cascaded to achieve high accuracy at the expense of increased simulation time that is prohibitively expensive in the parasitic-aware paradigm. The ABCD matrix method also provides significantly lower compact model circuit complexity.

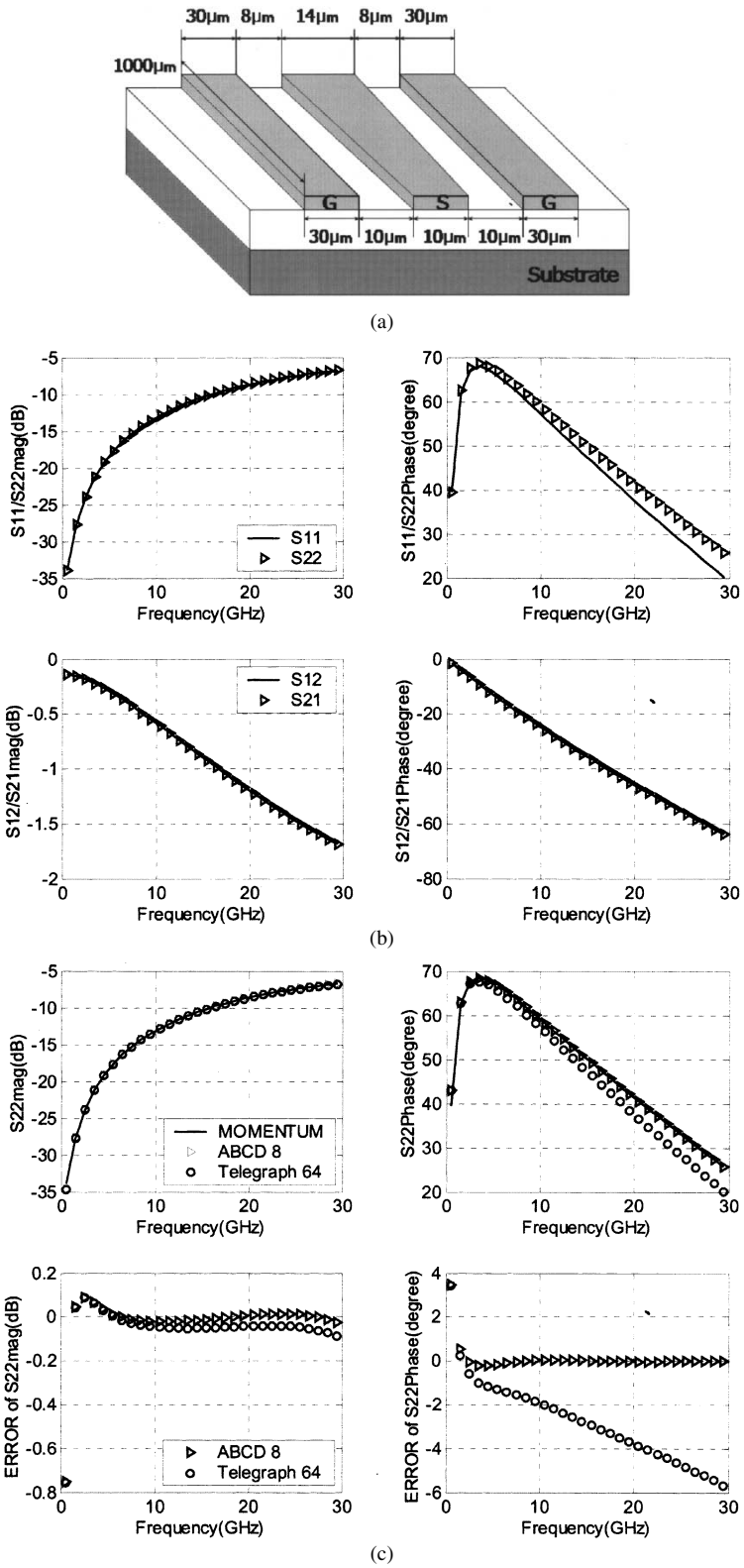

Fig. 5. (a) Asymmetric coplanar waveguide with $Ws\ (\text{port}\ 1) = 10\ \mu\text{m}$, $Ws\ (\text{port}\ 2) = 14\ \mu\text{m}$, $Sp = 10\ \mu\text{m}$, $Wg = 30\ \mu\text{m}$, and $L = 1000\ \mu\text{m}$. (b) Two-port characteristics of the asymmetric CPW showing significant phase differences between S_{11} and S_{22}. (c) Comparisons between the ABCD matrix and Telegrapher models for the magnitude and phase of S_{22}. The ABCD method accurately models the moderate asymmetric behavior using only eight asymmetric cells, whereas the Telegrapher method is inaccurate even with 64 cells owing to its inherent symmetry.

III. Distributed Circuit Model Extraction

The methodology for generating compact models begins with extraction of distributed circuit models from measured S-parameters for a small set of transmission lines spanning wide ranges of design parameter values as depicted in Fig. 1. A key next step is using the measured data to "calibrate" *MOMENTUM* so that measured and simulated results agree

prior to subsequent simulations. In the calibration process, the physically defined technology substrate definition input to *MOMENTUM* is empirically adjusted (e.g., substrate resistivity increased by 40 $\times$) [18]. The calibrated EM simulator is then used to generate accurate S-parameters for several transmission lines interpolated among the measured points (Fig. 1). Finally, compact models are extracted from the measured and calibrated EM simulated data and used to train a neural network to accurately and quickly generate compact models for *arbitrary* parameter values within the ranges bounded by the measured points. As with other fitting approaches, model accuracy is not guaranteed for parameter values outside the training boundaries.

An ABCD matrix partitioning procedure accurately and efficiently partitions transmission lines into distributed identical asymmetric T-cell sections. It takes advantage of an important property of ABCD matrices: When two identical distributed circuit sections are cascaded, the overall ABCD matrix is the square of the individual ABCD matrices; that is

$$[\mathbf{ABCD}]_T = [\mathbf{abcd}]_I^2 \tag{10}$$

where $[\mathbf{ABCD}]_T$ and $[\mathbf{abcd}]_I$ are the total and individual ABCD matrices, respectively. Another advantage is that ABCD parameters describe a two-port network in terms of voltages and currents, and are therefore inherently compatible with circuit simulators.

Converting measured or simulated S-parameter data into equivalent ABCD matrices is the first step in extracting the frequency-dependent lumped element values for the distributed T-cell sections (Fig. 4). Note that since the S-parameters include a reverse current component in addition to a forward current term, extraction from the ABCD matrix results in an asymmetric T-cell, in contrast to the symmetric cell extracted using the Telegrapher equations.

To demonstrate the usefulness of the asymmetric ABCD matrix cell, consider the tapered asymmetric coplanar waveguide shown in Fig. 5(a) with its calibrated *MOMENTUM* simulated S-parameters in Fig. 5(b). Note from Fig. 5(c) that only eight asymmetric ABCD matrix cells are needed to accurately fit the phase ofS_{22}; the symmetric model from the Telegraph equation simply cannot model the asymmetry. Note that neither method accurately models transmission lines with large asymmetries between the two ports.

The next key observation is that the square root of the overall ABCD matrix $[\mathbf{ABCD}]_T$, corresponds to a partitioning into two identical asymmetric T-cells, $[\mathbf{abcd}]_2$. Continuing, the square root of $[\mathbf{abcd}]_2$ produces four identical cells, $[\mathbf{abcd}]_4$, the square root of $[\mathbf{abcd}]_4$ produces eight identical cells, $[\mathbf{abcd}]_8$, and so on. This iterative characteristic underpins the transmission-line distributed circuit extraction algorithm. Specifically, iterating the square root $n = \log_2(N)$ times partitions the transmission line into N identical segments $[\mathbf{abcd}]_N$, where N is a power of two. Taking the square root of the complex ABCD matrix is done using the ***sqrtm***() function in *MATLAB*.

To illustrate the iterative process described above, consider a simple example. Fig. 6(a) lists S-parameter values from calibrated *MOMENTUM* simulations from 1 GHz to 30 GHz for a symmetric coplanar waveguide with $Ws = 10\ \mu$m, $Sp = 10\ \mu$m, $Wg = 30\ \mu$m, and $L = 1000\ \mu$m. For the 10-GHz frequency point, for example, the S-parameter matrix is converted to an equivalent ABCD matrix using the following relationships [15]:

Frequency	$\begin{bmatrix} S11 & S12 \\ S21 & S22 \end{bmatrix}$
1GHz	$\begin{bmatrix} 0.0196 + 0.0283j & 0.9800 - 0.0486j \\ 0.9800 - 0.0486j & 0.0196 + 0.0283j \end{bmatrix}$
10GHz	$\begin{bmatrix} 0.1362 + 0.2096j & 0.8329 - 0.4015j \\ 0.8329 - 0.4015j & 0.1362 + 0.2096j \end{bmatrix}$
20GHz	$\begin{bmatrix} 0.3252 + 0.2551j & 0.5798 - 0.6207j \\ 0.5798 - 0.6207j & 0.3252 + 0.2551j \end{bmatrix}$
30GHz	$\begin{bmatrix} 0.4752 + 0.1838j & 0.3294 - 0.7207j \\ 0.3294 - 0.7207j & 0.4752 + 0.1837j \end{bmatrix}$

(a)

$\begin{bmatrix} S11 & S12 \\ S21 & S22 \end{bmatrix}$	$\begin{bmatrix} 0.1362 + 0.2096j & 0.8329 - 0.4015j \\ 0.8329 - 0.4015j & 0.1362 + 0.2096j \end{bmatrix}$
$\begin{bmatrix} ABCD \end{bmatrix}$	$\begin{bmatrix} 0.9294 + 0.0122j & 3.9602 + 36.2784j \\ 0.0002 + 0.0038j & 0.9294 + 0.0122j \end{bmatrix}$
$\begin{bmatrix} abcd \end{bmatrix}_2$	$\begin{bmatrix} 0.9822 + 0.0031j & 2.0743 + 18.4616j \\ 0.0001 + 0.0019j & 0.9822 + 0.0031j \end{bmatrix}$
$\begin{bmatrix} abcd \end{bmatrix}_4$	$\begin{bmatrix} 0.9955 + 0.0008j & 1.0491 + 9.2714j \\ 0.0001 + 0.0010j & 0.9955 + 0.0008j \end{bmatrix}$
$\begin{bmatrix} abcd \end{bmatrix}_8$	$\begin{bmatrix} 0.9989 + 0.0002j & 0.5260 + 4.6408j \\ 0.0000 + 0.0005j & 0.9989 + 0.0002j \end{bmatrix}$

(b)

Fig. 6. (a) Simulated S-parameter in *MOMENTUM* from 1 to 30 GHz for a coplanar waveguide with $Ws = 10\,\mu$m, $Sp = 10\,\mu$m, $Wg = 30\,\mu$m, and $L = 1000\ \mu$m. (b) Details on the ABCD partition process with example at 10 GHz for a coplanar waveguide with $Ws = 10\ \mu$m, $Sp = 10\ \mu$m, $Wg = 30\ \mu$m, and $L = 1000\ \mu$m. (Note that $N = 8$ in this example).

$$\begin{aligned} A &= \frac{(1+S_{11})(1-S_{22})+S_{12}S_{21}}{2S_{21}} \\ B &= \frac{(1+S_{11})(1+S_{22})-S_{12}S_{21}}{2S_{21}} \cdot Z_0 \\ C &= \frac{(1-S_{11})(1-S_{22})-S_{12}S_{21}}{2S_{21}} \cdot \frac{1}{Z_0} \\ D &= \frac{(1-S_{11})(1+S_{22})+S_{12}S_{21}}{2S_{21}}. \end{aligned} \tag{11}$$

Then, the square root of the ABCD matrix, $[\mathbf{abcd}]_2$ is calculated, which means that the T line is partitioned into a cascade of two identical sections (Fig. 4). This procedure three times to partition the transmission line into a cascade of eight identical

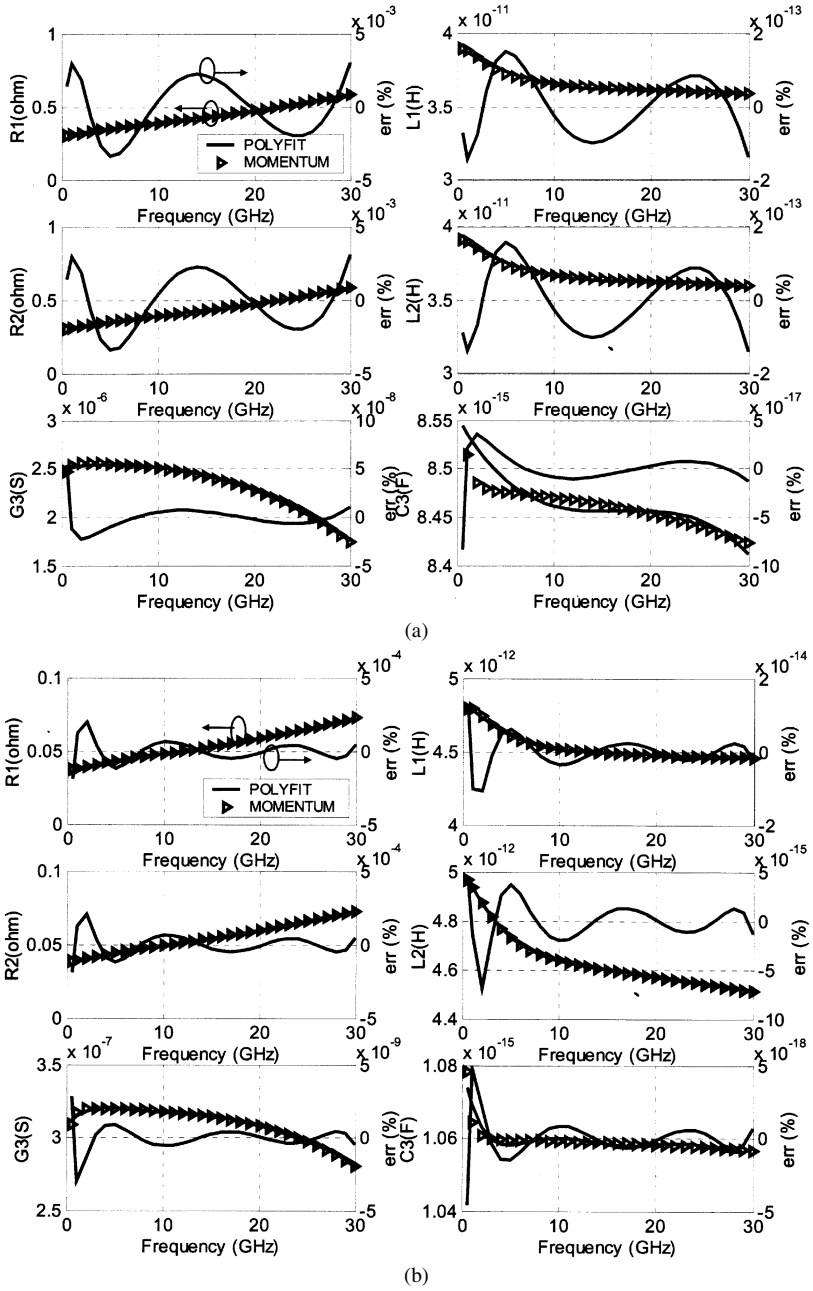

Fig. 7. Frequency-dependent component values for the T-cell. Each of the six T-cell element values is specified using a third-order frequency-dependent polynomial function. The T-cell is not symmetric; e.g., $L_1(f) \neq L_2(f)$, etc. Coplanar waveguide dimensions are $Ws = 10\ \mu$m, $Sp = 10\ \mu$m, $Wg = 30\ \mu$m, and $L = 1000\ \mu$m. (a) $N = 8$ T-cell sections. (b) 64 T-cell sections.

sections. Fig. 6(b) shows the details of the ABCD matrix partitioning process at 10 GHz where

$$[\mathbf{abcd}]_2 \times [\mathbf{abcd}]_2 = [\mathbf{ABCD}]$$
$$[\mathbf{abcd}]_4 \times [\mathbf{abcd}]_4 = [\mathbf{abcd}]_2$$
$$[\mathbf{abcd}]_8 \times [\mathbf{abcd}]_8 = [\mathbf{abcd}]_4. \tag{12}$$

After partitioning to the specified level of accuracy, the resulting unit matrix $[\mathbf{abcd}]_N$ is converted to the corresponding asymmetric T-cell. For each branch of the T-cell, the data are divided into real and imaginary components. The real component is fitted to an equivalent resistance $R(\omega)$ and the imaginary component is fitted to an equivalent inductance $L(\omega)$ or capacitance $C(\omega)$, depending on the branch. A standard curve-fitting technique is used to find the frequency-dependent element values of the T-cell. Specifically, a third-order polynomial function of frequency uses four coefficients to represent each of the six independent frequency-dependent components (Fig. 4). Hence, 24 coefficients determine the *netlist* corresponding to a T-cell; N identical T-cells are then cascaded to model the transmission line. Finally, the complete *HSPICE* netlist corresponding to the 24 coefficients for each of the N identical T-cells is simulated, and the resulting S-parameters are compared to their measured or calibrated *MOMENTUM* counterparts. An overview of the compact model extraction procedure is presented in Fig. 4. Typical curve fitting versus calibrated *MOMENTUM* results for the frequency-dependent T-cell element values are presented in Fig. 7.

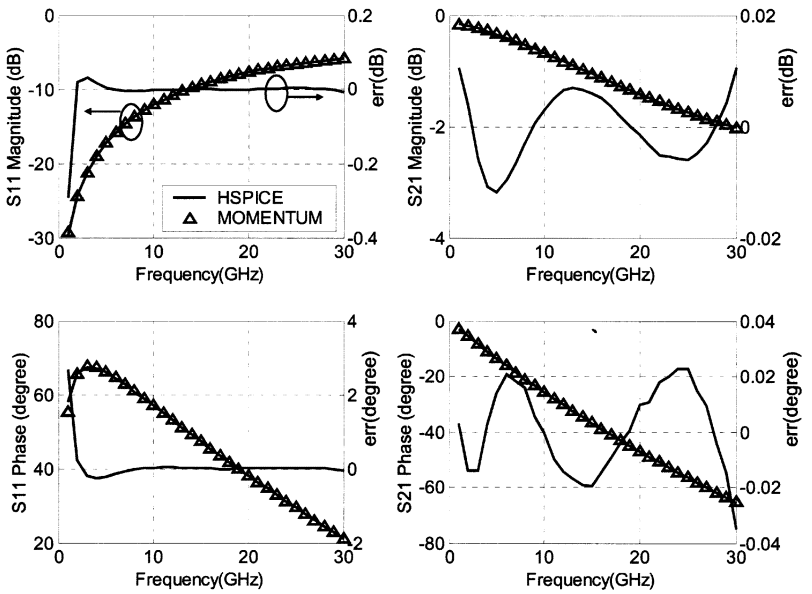

Fig. 8. Simulated *HSPICE* S-parameters for an $N = 8$ distributed T-cell model extracted using the ABCD matrix method compared with calibrated *MOMENTUM* S-parameters. Coplanar waveguide with $Ws = 10\ \mu$m, $Sp = 10\ \mu$m, $Wg = 30\ \mu$m, and $L = 1000\ \mu$m.

TABLE I
CMOS TECHNOLOGY PARAMETERS

Parameter	Value
Substrate Thickness	400μm
Substrate Dielectric Constant	11.7
Oxide Thickness (Below Layer 6)	10.3μm
SiO_2 Dielectric Constant	3.9
Top Metal (Layer 6) Thickness	1.8μm
Substrate Resistivity	10Ω·cm
Metal Conductivity	3.8×10^{-7}S/m

TABLE II
ERROR PERFORMANCE OF ABCD MATRIX METHOD (FIG. 8) ($Ws = 10\ \mu$m, $Sp = 10\ \mu$m, $Wg = 30\ \mu$m, $L = 1000\ \mu$m, AND $N = 8$)

S-parameter	$\lvert S_{11}\rvert$ (dB)	$\angle S_{11}$ (°)	$\lvert S_{21}\rvert$ (dB)	$\angle S_{21}$ (°)
Mean Error	0.0139	0.1391	0.0052	0.0133
Max Error	0.2992	2.6959	0.0119	0.0350

Many transmission-line structures have been simulated using calibrated *MOMENTUM* to validate the ABCD matrix method. The technology parameters used in *MOMENTUM* for a 1–30-GHz range of frequencies are summarized in Table I; the CMOS process has a one polysilicon layer and six metal layers; all transmission lines use the top metal (layer 6) with 1.8-μm thickness. Excellent agreement is achieved (Fig. 8) between calibrated *MOMENTUM* S-parameters of a coplanar waveguide and *HSPICE* simulations of a cascade of only $N = 8$ identical T-cells. Detailed error performance is plotted in Fig. 8 and summarized in Table II.

As exemplified in Fig. 9 for the magnitude of S_{11}, the ABCD matrix method needs far fewer T-cell sections than the Telegrapher technique for similar compact model accuracy; e.g., the ABCD matrix method uses only four asymmetric T-cells to match the accuracy of the Telegrapher method using 32 symmetrical T-cells. In general, the ABCD matrix method accommodates moderate transmission line asymmetries and achieves high accuracy with simpler compact circuit models.

IV. NEURAL-NETWORK MODELS

The compact model distributed element values of a transmission line are functions of its structure, design parameter values, and frequency. Since it is practical to fabricate only a few transmission lines for a design library (Fig. 1), a fast and accurate compact model generator for arbitrary sizes within the training boundaries is required for parasitic-aware design and optimization. To minimize computation, the compact model must be simple; e.g., *MOMENTUM* simulations show that coplanar waveguide S-parameters depend strongly on Ws, Sp, L, and frequency, but weakly on Wg. Hence, $Wg \approx 3Ws$ is assumed herein without loss of generality.

Attention now turns to the fast and accurate generation of compact distributed circuit models; i.e., determination of the 24 polynomial coefficients for coplanar waveguide T-cell sections with arbitrary Ws, Sp, and L, parameter values. From a high-level viewpoint, the task amounts to a nonlinear multiinput multioutput mapping problem. Since neural networks are known to provide powerful interpolation capabilities for such problems [19], it is appropriate to consider them for generating compact transmission-line models [20]. Owing to the nonlinear nature of the problem, a multilayer feedforward neural network is used with an input layer, an output layer, and one (or more) hidden layers as shown in Fig. 10(a). Each layer comprises several computation nodes (neurons) as detailed in Fig. 10(b). Different connections of neurons specify different architectures. In the feedforward network, for example, the inputs to neurons in a given layer are linked only to outputs of neurons in the preceding layer. Fractional inputs are specified using weighting coefficients, and a bias coefficient is applied to an entire layer. Summation of the weighted inputs to each neuron is affected

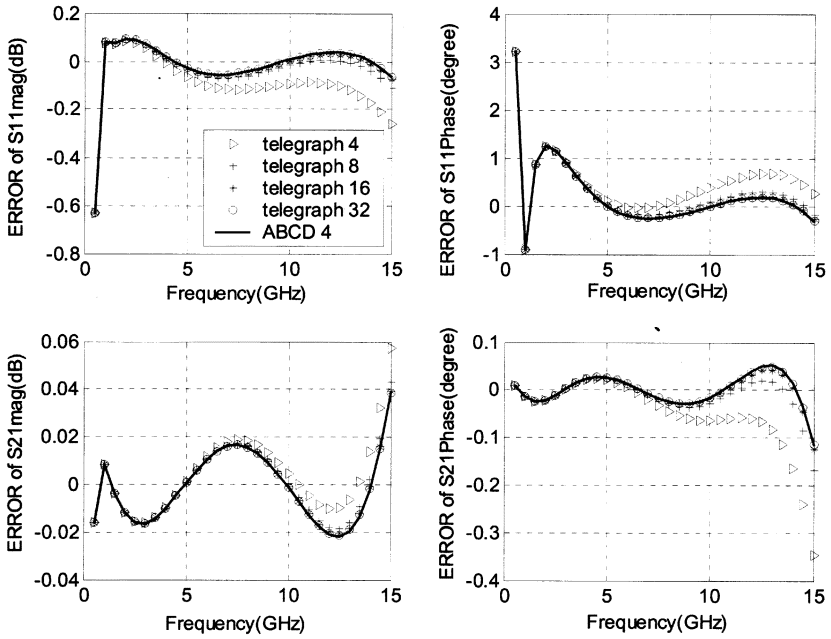

Fig. 9. Modeling accuracy versus the number of distributed T-cell segments for the magnitude of S_{11}. Excellent agreement with calibrated *MOMENTUM* results is obtained cascading only four identical asymmetric T-cell sections extracted using the ABCD matrix method versus 32 symmetric sections with the Telegrapher approach. Coplanar waveguide with $Ws = 10\ \mu$m, $Sp = 10\ \mu$m, $Wg = 30\ \mu$m, and $L = 1000\ \mu$m.

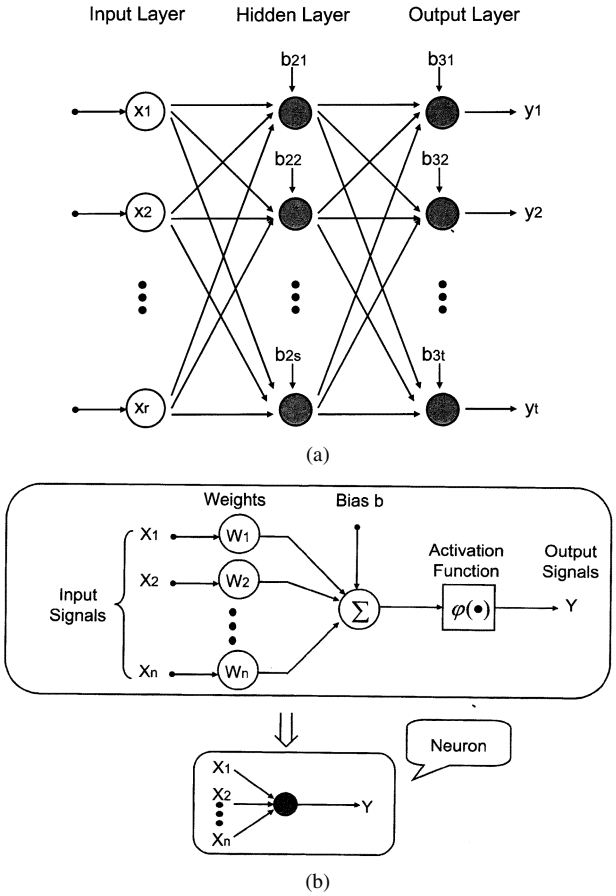

Fig. 10. (a) An r-s-t feedforward neural network has one input layer with r nodes, one hidden layer with s neurons, and one output layer with t nodes, where r, s, and t are integers. (b) Detailed definition of a neuron or computation node.

by a nonlinear activation function. In modeling coplanar waveguides, the input layer typically has three computation nodes corresponding to design parameters Ws, Sp, and L, and the output layer has four neurons representing the third-order polynomial fitting coefficients. Six independent neural networks of the type shown in Fig. 10(a) are used to generate the four fitting coefficients for each of the six frequency-dependent element values $R_1(\omega)$, $L_1(\omega)$, $R_2(\omega)$, $L_2(\omega)$, $G_3(\omega)$, and $C_3(\omega)$. Note that the numbers of hidden layers and nodes in each are determined empirically from simulations to achieve the desired accuracy. In general (Fig. 10(a)), there is one input layer with r nodes, one hidden layer with s neurons, and one output layer with t nodes, where r, s, and t are integers; hence, this architecture is termed an r-s-t structure. Table III gives the r-s-t structural details and activation functions used for each of the six independent neural networks.

TABLE III
ANN STRUCTURES FOR CIRCUIT COMPONENTS AND ACTIVATION FUNCTIONS

Circuit Components	ANN r-s-t Structure	Activation Functions
$R_1(\omega)$	3-8-4	$f_h(x) = \tanh(x)$ $f_o(x) = x$
$L_1(\omega)$	3-6-4	$f_h(x) = \tanh(x)$ $f_o(x) = x$
$R_2(\omega)$	3-8-4	$f_h(x) = \tanh(x)$ $f_o(x) = x$
$L_2(\omega)$	3-6-4	$f_h(x) = \tanh(x)$ $f_o(x) = x$
$G_3(\omega)$	3-8-4	$f_h(x) = \tanh(x)$ $f_o(x) = x$
$C_3(\omega)$	3-8-4	$f_h(x) = \tanh(x)$ $f_o(x) = x$

Before the neural network is used for compact model generation in the parasitic-aware optimization loop, it is trained using a database extracted by the ABCD matrix method from measured data and calibrated *MOMENTUM* results. The ranges of design parameter values of the coplanar waveguides in the design library are selected to satisfy anticipated design requirements so

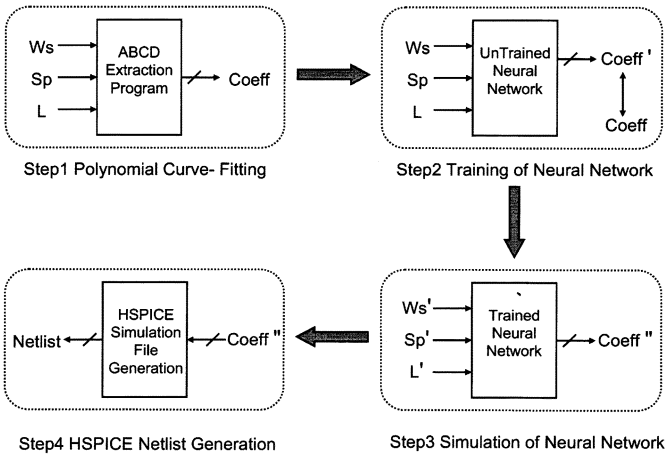

Fig. 11. ANN compact model generation methodology. The ABCD partitioning method is first used to extract compact models for a small set of measured and EM-simulated structures. After the feedforward ANN is subsequently trained, it interpolates to generate compact models for transmission lines with arbitrary sizes. Frequency information is implicit in the fitting coefficients, and not an explicit input variable.

that the neural network is used only in an interpolation mode during model generation.

The neural-network training procedure is now detailed. Suppose there exists a set of training vectors $\mathbf{D_i}(i = 1, 2, \ldots, N)$ where each $\mathbf{D_i}$ comprises an input data vector $\mathbf{X_i}$ and an output data vector $\mathbf{Y_i}$. Moreover, the input vector $\mathbf{X_i}$ applied to the untrained neural network produces output vector $\mathbf{Z_i}$; error vector $\mathbf{E_i}$ is defined as the difference between $\mathbf{Y_i}$ and $\mathbf{Z_i}$; the training algorithm tries to equalize $\mathbf{Z_i}$ to $\mathbf{Y_i}$ to minimize $\mathbf{E_i}$ for all $\mathbf{D_i}$. Training ends when the mean square error falls below a preset empirical value.

In our transmission-line compact model generator, a back-error propagation algorithm [21] is used to train the neural network. Consequently, the trained feedforward ANN is a generalization of the nonlinear mapping functions implicit in a limited training database. More specifically, due to the natural interpolation capabilities of the trained ANN, it is able to quickly produce an output vector $\mathbf{Z_{new,j}}$ that closely approximates a target output $\mathbf{Y_{new,j}}$ when a new data point $\mathbf{X_{new,j}}$ is applied. In other words, the interpolation process in the trained ANN enables fast and accurate generation of the polynomial fitting coefficients for transmission lines with arbitrary parameter values. The overall model generation approach for the feedforward ANN trained using T-cell data extracted by the ABCD partitioning methodology is summarized in Fig. 11.

The extracted training data are also used to avoid the classical ANN over-training problem [22]. In the process flow illustrated in Fig. 11, the input vector is $\mathbf{X} = (Ws, Sp, L)$ and the output vector is $\mathbf{Y} = (c_0, c_1, c_2, c_3)$. Note that since the polynomial coefficients, $c_i(i = 0, 1, 2, 3)$, implicitly include frequency dependencies, it is not necessary to include frequency as an explicit input variable. Since frequency information is effectively hidden, computation time is saved during execution of the training algorithm and subsequent compact model generation.

Fig. 12(a) details the new compact model generation procedure that combines the ABCD matrix partitioning procedure

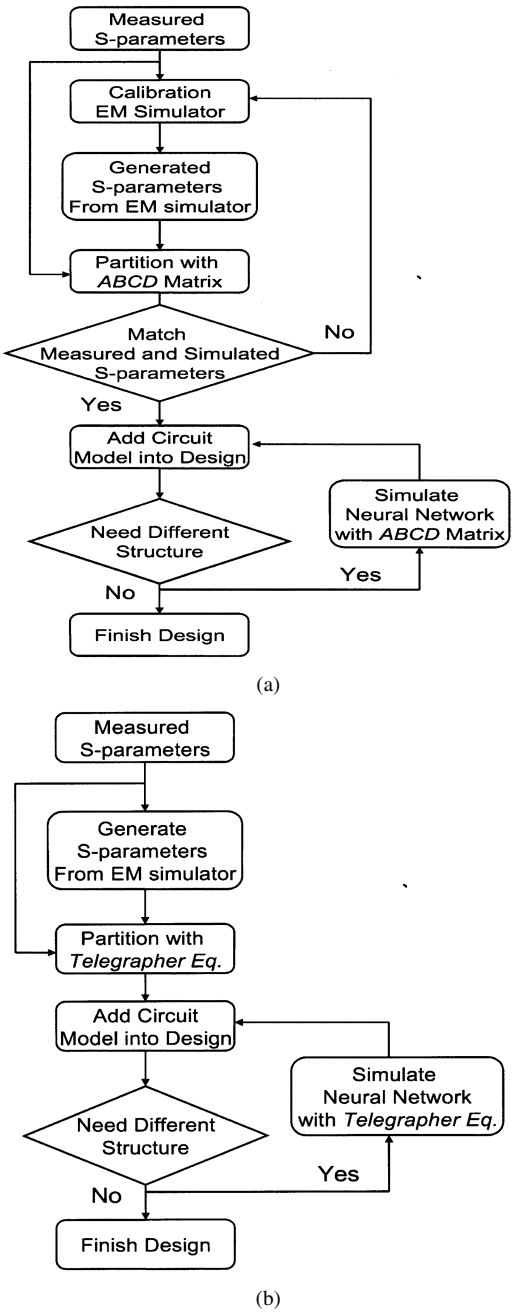

Fig. 12. (a) New compact model generation methodology combines the ABCD partitioning technique and the trained feedforward trained neural network. (b) Telegrapher equation design flow is slower due to EM simulations that are required during parasitic-aware optimization.

with the trained feedforward ANN. For comparison, Fig. 12(b) depicts the conventional method of compact model generation using the Telegrapher equations. Accurate parasitic-aware RF circuit synthesis is accelerated using the proposed methodology because time-consuming EM simulations are not needed after the ANN is trained.

To validate the compact model generation methodology, a large set of neural network training data was first generated using calibrated *MOMENTUM* simulations and the ABCD matrix extraction method for 125 coplanar waveguides spanning the ranges of parameter values given in Table IV. The trained ANN was then used to generate compact models for 120

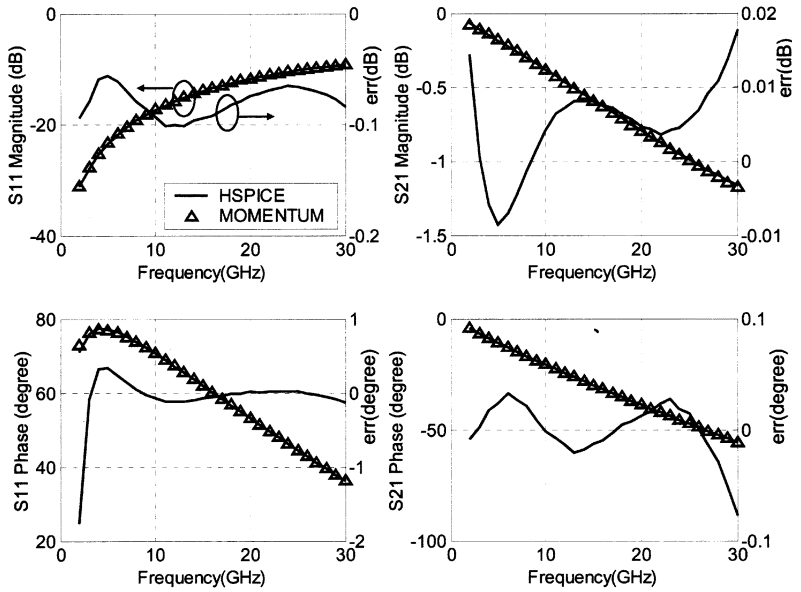

Fig. 13. S-parameters from *HSPICE* simulations of the compact circuit model generated by the ANN compared to calibrated *MOMENTUM* simulations with $Ws = 24\ \mu$m, $Sp = 18\ \mu$m, $Wg = 60\ \mu$m, and $L = 800\ \mu$m. $N = 8$ T-cell sections are used.

TABLE IV
PARAMETER RANGE FOR NEURAL NETWORK MODELS

Parameter	Min Value	Max Value
Freq. (GHz)	1	30
Ws (μm)	10	40
Sp (μm)	10	40
L (μm)	200	1000

TABLE V
ERROR PERFORMANCE OF NEURAL NETWORK MODEL

S-parameter	$\lvert S_{11}\rvert$ (dB)	$\angle S_{11}$ (°)	$\lvert S_{12}\rvert$ (dB)	$\angle S_{12}$ (°)
Mean Error	0.0454	0.2155	0.0033	0.0291
S-parameter	$\lvert S_{21}\rvert$ (dB)	$\angle S_{21}$ (°)	$\lvert S_{22}\rvert$ (dB)	$\angle S_{22}$ (°)
Mean Error	0.0033	0.0291	0.0459	0.2184

coplanar waveguides with arbitrary sizes within the parameter ranges. In practice, the process ends here. However, to access the accuracy of the ANN model generator, the same 120 coplanar waveguides were also simulated using calibrated *MOMENTUM*; the results were in close agreement with *HSPICE* simulations of the corresponding compact circuit models. Fig. 13 shows a typical set of results, and Table V shows the worst-case error performance from among the 120 verification examples. Of course, if higher accuracy is needed, the number of T-cells in the distributed compact model can be increased.

The ABCD matrix extraction technique in conjunction with the feedforward ANN easily handles three explicit parameters, Ws, Sp, and L, and one implicit parameter, frequency. However, there is potential concern about randomness owing to the nature of the training algorithm. It is plausible that the trained outcome of the neural network is different depending on the order in which the training data is applied. To assess this concern, the neural network training process was repeated several times using different training data sets applied in different orders. The ANN compact model generation methodology proved extremely robust in producing low error performance.

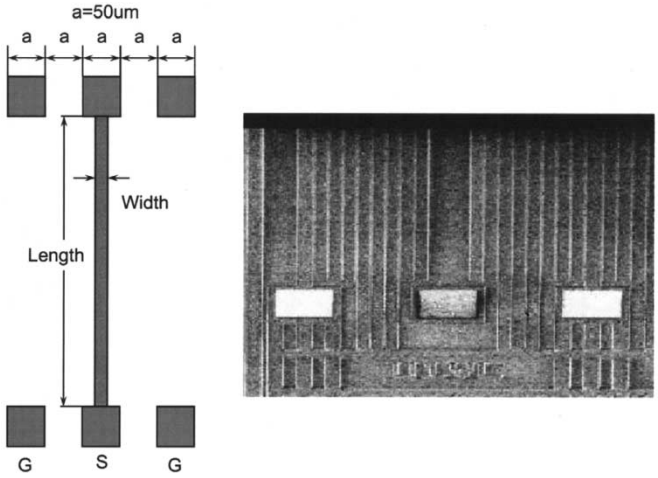

Fig. 14. Transmission-line structure. Six test structures with $L = 400\ \mu$m, 800 μm, and 6400 μm and $Ws = 0.6\ \mu$m and 0.7 μm were fabricated. (Microphotograph and measured results courtesy of M. B. Steer at North Carolina State University).

Training of the feedforward ANN using 125 sets of training data requires several minutes of computer time on a *Sun Ultra-10* Unix Workstation. However, since training is performed only once prior to parasitic-aware design and optimization, it presents no computational burden to the ANN compact model generator. In fact, the CPU time required to generate a distributed circuit model with eight unit T-cells for an arbitrary transmission line is less than 1 ms. Hence, the new compact model generator facilitates parasitic-aware optimization of complex RF circuits with transmission lines in a few hours of CPU time versus several days using conventional methods.

V. VERIFICATION WITH MEASURED RESULTS

To further verify the validity of the proposed compact modeling methodology, measurements were used from two sets of

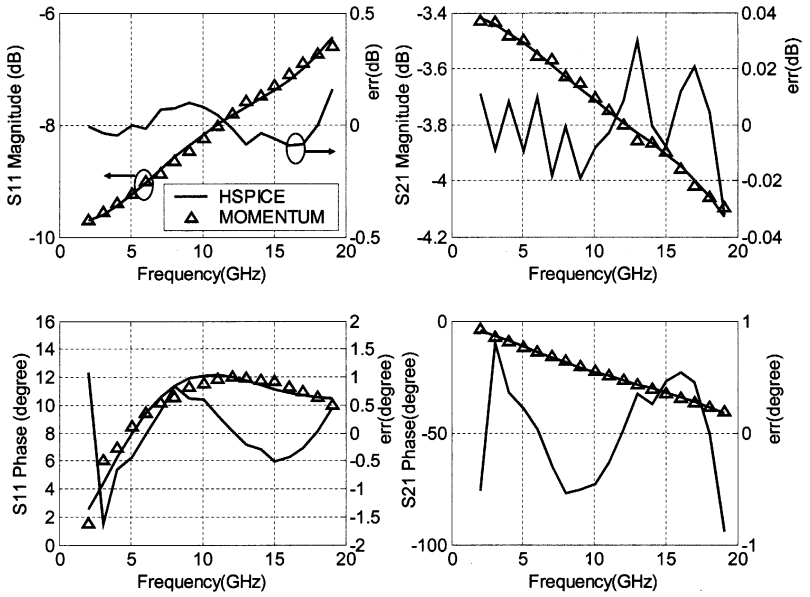

Fig. 15. S-parameters obtained from *HSPICE* simulations of a compact circuit model versus measured data of the same microstrip line structure with $Ws = 0.6\ \mu$m and $L = 800\mu$m. $N = 8$ T-cell sections are used.

microstrip lines fabricated in silicon with different signal widths (0.6 and 0.7 μm) [23], [24]. Each set included short (400-μm), medium (800-μm), and long (6400-μm) lines. Several characteristics were measured from 45 MHz to 20.045 GHz using an *HP 8510* network analyzer and *Picoprobe Model 40* probes. The electrical probe pads in the ground-signal-ground (GSG) configuration were 50-μm square with 100-μm pitch. The residual capacitance of the microprobe and probing pad (approximately 70 fF) was calibrated out. A test setup and partial chip microphotograph are shown in Fig. 14. An *HP 4275A* 10 MHz was used to measure capacitances of the transmission-line structures. Capacitance per meter length was calculated from the difference of the long and short line capacitance measurements divided by 0.0006 m. This value is then input into a calibration program; it collects arrays of rough calibration S-parameter data for each of the three structures in a given family, and automatically applies the through-line de-embedding algorithm [23] to determine the S-parameters of the embedded transmission lines. The characteristic impedance and propagation constant of the transmission lines are determined from the resistance R, inductance L, conductance G, and capacitance C-parameters per-unit length of the transmission lines as described earlier.

Fig. 15 shows *HSPICE* simulated S-parameters for a distributed circuit model with eight sections generated using the proposed compact modeling technique versus measured values. As shown, good agreement between the measured and simulated S-parameters is observed over the full range of measurement frequencies.

VI. Conclusions

A fast and accurate method for extracting distributed circuit T-cell compact models with frequency dependent components for on-chip transmission lines is presented in this paper. The extraction technique uses a novel ABCD matrix partitioning procedure to reduce compact model circuit complexity and increase accuracy compared to conventional extraction based on the Telegrapher equations. Moreover, the ABCD partitioning approach accurately handles both symmetric structures and those with moderate asymmetries due to layout, process, voltage, and temperature variations, etc. The compact models extracted from a small set of measured and simulated transmission lines spanning ranges of design parameter values are used to train a feedforward ANN. After training, the ANN accurately and efficiently generates compact circuit models for arbitrary transmission-line sizes within a parasitic-aware optimization loop. Extensive comparisons of *HSPICE* circuit simulations for the compact circuit models versus calibrated *MOMENTUM* results confirm the accuracy of the proposed methodology up to 30 GHz. Comparison of measured data versus models from the proposed method further confirms its validity. The transmission-line compact circuit model generator is readily integrated with various optimization programs and circuit simulators in parasitic-aware RF IC design and optimization tools.

Acknowledgment

The authors wish to thank Prof. M. B. Steer, S. Lipa, and B. Biswas, North Carolina State University, for providing the detailed layout information and S-parameter measurements used for verification.

References

[1] Q. Huang, F. Piazza, P. Orsatti, and T. Ohguro, "The impact of scaling down to deep submicron on CMOS RF circuits," *IEEE J. Solid-State Circuits*, vol. 33, pp. 1023–1036, July 1998.

[2] B. Razavi, "CMOS technology characterization for analog and RF design," *IEEE J. Solid-State Circuits*, vol. 34, pp. 268–276, Mar. 1999.

[3] T. H. Lee and S. S. Wong, "CMOS RF integrated circuits at 5 GHz and beyond," *Proc. IEEE*, vol. 88, pp. 1560–1571, Oct. 2000.

[4] H. Hasegawa, M. Furukawa, and H. Yanai, "Properties of microstrip line on Si- Si O_2 system," *IEEE Trans. Microwave Theory Tech.*, vol. MTT-19, pp. 869–881, Nov. 1971.

[5] E. Groteluschen, L. S. Dutta, and S. Zaage, "Full-wave analysis and analytical formulas for the line parameters of transmission lines on semiconductor substrates," *VLSI J.*, vol. 16, pp. 33–58, 1993.
[6] C. P. Wen, "Coplanar waveguide: A surface strip transmission line suitable for nonreciprocal gyromagnetic device applications," *IEEE Trans. Microwave Theory Tech.*, vol. MTT-17, pp. 1087–1090, Dec. 1969.
[7] C. Veyres and V. F. Hanna, "Extension of the application of conformal mapping techniques to coplanar lines with finite dimensions," *Int. J. Electron.*, vol. 48, pp. 47–56, 1980.
[8] E. Chen and S. Y. Chou, "Characteristics of coplanar transmission lines on multilayer substrates: Modeling and experiments," *IEEE Trans. Microwave Theory Tech.*, vol. 45, pp. 939–945, June 1997.
[9] V. Milanovic, M. Ozgur, D. C. DeGroot, J. A. Jargon, M. Gaitan, and M. E. Zaghloul, "Characterization of broad-band transmission for coplanar waveguides on CMOS silicon substrates," *IEEE Trans. Microwave Theory Tech.*, vol. 46, pp. 632–640, May 1998.
[10] A. Tripathi, Y.-C. Hahm, A. Weisshaar, and V. K. Tripathi, "Quasi-TEM spectral domain approach for calculating distributed inductance and resistance of microstrip on Si- Si O_2 substrate," *Electron. Lett.*, vol. 34, no. 13, pp. 1330–1331, June 1998.
[11] *Agilent EEsof Momentum, Electromagnetic Design and Simulation, Advanced Design System 1.5*, Agilent Technologies, Palo Alto, CA, 2000.
[12] R. Gupta and D. J. Allstot, "Parasitic-aware design and optimization of CMOS RF integrated circuits," in *Proc. IEEE Radio Frequency Integrated Circuits Symp.*, 1998, pp. 325–328.
[13] ——, "Parasitic-aware design and optimization of CMOS RF integrated circuits," in *Proc. IEEE MTT-S Int. Microwave Symp.*, vol. 3, 1998, pp. 1867–1870.
[14] K. Choi, J. Park, and D. J. Allstot, *Parasitic-Aware RF Circuit Optimization*. Boston, MA: Kluwer, 2003.
[15] D. M. Pozar, *Microwave Engineering*, 2nd ed. New York: Wiley, 1998.
[16] W. R. Eisenstadt and Y. Eo, "S-parameter-based IC interconnect transmission line characterization," *IEEE Trans. Comp., Hybrids, Manufact. Technol.*, vol. 15, pp. 483–490, Aug. 1992.
[17] Y. Eo and W. R. Eisenstadt, "High-speed VLSI interconnect modeling based on S-parameter measurements," *IEEE Trans. Comp., Hybrids, Manufact. Technol.*, vol. 16, pp. 555–562, Aug. 1993.
[18] D. J. Allstot, B. M. Ballweber, and R. Gupta, "CMOS distributed amplifier design using CAD optimization techniques," in *Proc. Southwest Symp. Mixed-Signal Design*, 1999, pp. 140–146.
[19] G. Van der Plas, J. Vandenbussche, G. Gielen, and W. Sansen, "EsteMate: A tool for automated power and area estimation in analog top-down design and synthesis," in *Proc. IEEE Custom Integrated Circuits Conf.*, 1997, pp. 139–142.
[20] P. M. Watson and K. C. Gupta, "Design and optimization of transmission-line circuits using EM-ANN models for transmission-line components," *IEEE Trans. Microwave Theory Tech.*, vol. 45, pp. 2515–2523, Dec. 1997.
[21] L. V. Fausett, *Fundamentals of Neural Networks: Architectures, Algorithms and Applications*. Englewood Cliffs, NJ: Prentice-Hall, 1994.
[22] S. Haykin, *Neural Networks: A Comprehensive Foundation*, 2nd ed. Englewood Cliffs, NJ: Prentice-Hall, 1999.
[23] S. Lipa, M. B. Steer, A. C. Cangellaris, and P. D. Franzon, "Experimental characterization of transmission lines in thin-film multichip modules," *IEEE Trans. Comp., Packag., Manufact. Technol.*, pt. A, vol. 19, pp. 122–126, Mar. 1996.
[24] B. Biswas, "Modeling and simulation of high speed interconnects," M.S.E.E. thesis, Dept. Elect. Eng., North Carolina State Univ., Raleigh, 1998.

Taeik Kim (S'01) received the B.S. and M.S. degrees in electrical engineering from Korea University, Seoul, Korea, in 1991, and 1996, respectively. He is currently working toward the Ph.D. degree in electrical engineering at the University of Washington, Seattle.

In 2000, he was with the Desktop Platform Group, Intel, Santa Clara, CA, where he developed and designed high-speed I/O circuits. His current research work is in RF analog and mixed-signal circuits for wireless communications, including voltage-controlled oscillators and phase shifters.

Xiaoyong Li (S'01) was born in Shannxi, China. He received the B.S. and M.S. degrees (with highest honors) from Peking University, Beijing, China, in 1997 and 2000, respectively. He is currently working toward the Ph.D. degree in the Department of Electrical Engineering, University of Washington, Seattle.

His research interests are in the analysis and design of mixed signal integrated circuits and radio frequency integrated circuits.

Mr. Li received the Motorola Scholarship, P&G Scholarship and Kodak Scholarship at Peking University in 1996, 1997 and 1999, respectively. He was awarded the Analog Devices Outstanding Student Designer Award in 2002.

David J. Allstot (S'72–M'72–SM'83–F'92) received the B.S., degree from the University of Portland, Portland, OR, the M.S. degree from the Oregon State University, Corvallis, and the Ph.D. degree from the University of California, Berkeley, respectively.

He has held several industrial and academic positions and has been the Boeing-Egtvedt Chair Professor of Engineering at the University of Washington since 1999. He has advised approximately 75 M.S. and Ph.D. graduates and published about 175 papers.

Dr. Allstot is the recipient of several awards, including the 1978 IEEE W.R.G. Baker Prize Paper Award, the 1995 IEEE Circuits and Systems Society Darlington Best Paper Award, the 1998 IEEE International Solid-State Circuits Conference Beatrice Winner Award, the 1999 IEEE Circuits and Systems Society Golden Jubilee Medal, and the 2000 International Solid-State Circuits Conference Outstanding Service Award. He was an Associate Editor of IEEE TRANSACTIONS ON CIRCUITS AND SYSTEMS—II: ANALOG AND DIGITAL SIGNAL PROCESSING from 1990 to 1993, and its Editor from 1993 to 1995. He has served on the Technical Program Committee, IEEE Custom IC Conference, from 1990 to 1993, on the Education Award Committee, IEEE Circuits and Systems Society, from 1990 to 1993, on the Board of Governors, IEEE Circuits and Systems Society, from 1992 to 1995, on the Technical Program Committee, IEEE International Symposium on Low-Power Electronics and Design from 1994 to 1997, on the Mac Van Valkenberg Award Committee, IEEE Circuits and Systems Society, from 1994 to 1996, and since 1994 is serving on the Technical Program Committee, IEEE International Solid-State Circuits Conference. He has been the 1995 Special Sessions Chair, IEEE International Symposium on Circuits and Systems, the Executive Committee Member and Short Course Chair, IEEE International Solid-State Circuits Conference, from 1996 to 2000, the Co-Chair, IEEE Solid-State Circuits and Technology Committee, from 1996 to 1998, Distinguished Lecturer, IEEE Circuits and Systems Society, from 2000 to 2001, and the Co-General Chair, IEEE International Symposium on Circuits and Systems in 2002. He is a Member of Eta Kappa Nu and Sigma Xi.